International Journal of Multiphase Flow 174 (2024) 104754

Contents lists available at ScienceDirect

International Journal of Multiphase Flow

journal homepage: www.elsevier.com/locate/ijmulflow

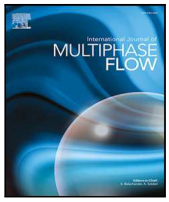

A computational study on the effect of particle characteristics on the deposition of small particles in turbulent wall-bounded flows

S. Abbasi, A. Mehdizadeh *

School of Science and Engineering, University of Missouri – Kansas City, MO, USA

ARTICLE INFO

Keywords:
Turbulent dispersed channel flow
Direct numerical simulation
Lagrangian particle tracking
Wall boundary correction
Deposition

ABSTRACT

Particle deposition dynamics in a fully developed turbulent channel flow at a friction Reynolds number of $Re_\tau = 180$ for two Stokes numbers ($St = 1$ and 10) are investigated using the point particle-direct numerical simulation (PP-DNS) method, considering dilute system and thus, one-way coupling. In particular, the interplay between particle size, particle property (density) and deposition at the same Stokes number has been investigated. It turns out that the dimensionless particle relaxation time (the Stokes number) alone does not provide enough information to capture the deposition dynamics, and particle size (diameter) and density need to be considered to obtain a more comprehensive understanding of deposition process. Furthermore, we demonstrate that gravity significantly alter the deposition patterns of particles with different size and density differently, even if the Stokes number does not change, and therefore the results from zero gravity cannot be extrapolated to non-zero gravity settings, even for small particles. Finally, our results suggest that wall-normal particle velocity variance at the wall plays an integral role in the deposition process, as it approaches a finite value (significantly larger than particle mean velocity) at the wall.

1. Introduction

Particle transport and deposition in wall-bounded turbulent flows has been the focus of many studies because of its appearance in various industrial or environmental systems (Alimohammadi et al., 2019; Lu and Wang, 2019; Alcoforado et al., 2019; Bui et al., 2020; Sommerfeld et al., 2021). Particularly, deposition of small particles is a fundamental issue in many emerging and conventional industries including unconventional geothermal systems (Chauhan, 2019; Chauhan et al., 2020), biomass conversion systems (Cai et al., 2018; Kleinhans et al., 2018), petroleum and petrochemical industries (Santos, 2009; Paes et al., 2015; Gharbi et al., 2017), modern gas turbines in power-generating facilities (Healy and Young, 2010; Kurz and Brun, 2012), to name only a few. Therefore, understanding the mechanisms of this phenomenon is of importance to help reduce its negative economical and environmental effects. However, the complexity of the deposition process makes it a formidable challenge that has not yet been completely addressed, even when generic configurations such as channel flow that allow for application of high-fidelity methods, are considered.

The rate of the number of particles depositing on a wall is usually referred to as deposition velocity (u_d^+) and expressed as a function of dimensionless particle response time, i.e. the Stokes number (St). Young and Leeming (1997) have gathered various experimental data from turbulent pipe/duct flows in Fig. 1. The deposition plot is generally divided into three regimes; for small Stokes numbers in diffusional deposition regime, deposition is primarily driven by turbulent diffusion in the core of the flow and then by Brownian motion adjacent to the wall. With increase in the Stokes number, particle's inertia becomes significant and its interaction with turbulent eddies results in a substantial increase of deposition rate, i.e. diffusion-impaction regime. In the inertia-moderated regime, diffusion plays a little part in deposition and particle's response to the turbulence decreases, which reduces the deposition rate (Young and Leeming, 1997). Thus the dominant mechanism for the deposition of small particles is the turbulent diffusion (diffusional deposition regime) and for particles with higher inertia (diffusional-impaction and inertia-moderated regimes) is the convective drift of particles towards the wall due to the gradient in the turbulent intensity, denoted typically as "Turbophoresis".

Yet, the scattered nature of the experimental data on deposition velocity (rate) shown in Fig. 1 (note that deposition velocity is plotted on a logarithmic scale), suggests that the deposition rate may not be solely a function of the particle Stokes number. Deposition velocity could depend on other non-dimensional parameters, such as the ratio of the particle diameter to the Kolmogorov length scale and/or the particle-to-fluid density ratio. For example, the experiments of Friedlander and Johnstone (1957) and Sehmel (1968) have the same setup, i.e. same

* Corresponding author.
E-mail addresses: sa8x5@umkc.edu (S. Abbasi), mehdizadeha@umkc.edu (A. Mehdizadeh).

https://doi.org/10.1016/j.ijmultiphaseflow.2024.104754
Received 17 July 2023; Received in revised form 19 January 2024; Accepted 2 February 2024
Available online 8 February 2024

Nomenclature

Greek letters

δ	Constant source
ϵ	Finite shear rate
γ	Stretching factor
ν	Fluid viscosity
ρ	Fluid density
τ	Time scale, shear stress
$\boldsymbol{\omega}$	Vorticity

Latin symbols

$\mathbf{a}$	Acceleration
C	Concentration, constant, coefficient
d	Diameter
$\mathbf{g}$	Gravitational acceleration
H	Height
h	Channel half height
J	Flux, lift correction
L	Length
l	Distance
N	Number
p	Pressure
Re	Reynolds number
Re_τ	Friction Reynolds number
$\mathbf{r}$	Particle position
s	Slab
St	Stokes number
t	Time
$\mathbf{u}$	Fluid velocity
u	Velocity
u_τ	Friction velocity at the wall
U	Streamwise velocity
$\mathbf{v}$	Particle velocity
W	Wall-normal velocity, width
x	Streamwise direction
y	spanwise direction
z	Wall-normal direction

Subscripts/Superscripts

τ	Shear stress
d/dep	Deposition
D/G/L	Drag/gravity/lift
f	Fluid
i	Index
p	Particle
rms	Root mean square
W	Wall correction
0	Initial value
$+$ /$*$	Dimensionless variable
$\perp$	Perpendicular to wall
$\parallel$	Parallel to wall
$\langle\,\rangle$	Averaged

List of abbreviations

DNS	Direct numerical simulation
LES	Large eddy simulation
LPT	Lagrangian particle tracking
RANS	Reynolds-averaged Navier–Stokes
RMS	Root mean square

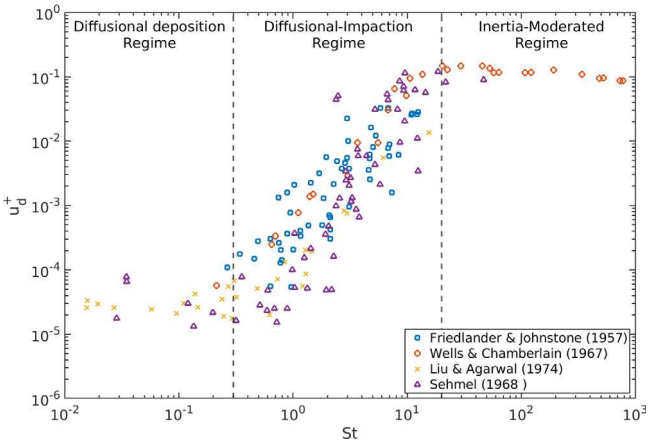

Fig. 1. A summary of particle deposition velocities w.r.t. Stokes number obtained from experimental measurements. The plot is taken from Young and Leeming (1997).

pipe diameter and Reynolds number, but use different materials and particle sizes at the same Stokes numbers, and their obtained deposition velocities have at least one order of magnitude difference. Therefore, reliable models are needed for study of dispersion and deposition process in complex configurations relevant to industrial applications as conducting high-fidelity simulations for every single setting is (computationally) prohibitively expensive, even for very generic flows such as channel flow.

Particle deposition in turbulent channel flow was first investigated by McLaughlin (1989) by means of point particle-direct numerical simulation (PP-DNS) method. However, there are some limitations to the study that might pose some uncertainties. In particular, the equation of particle motion did not include wall-correction to either drag or lift, which are relevant to the deposition process (Molin et al., 2012). Later, Chen and McLaughlin (1995) investigated the deposition dynamics in the channel flow considering the near-wall corrections for drag and lift. It was shown that the deposition is a function of particle diameter and Stokes number. This study, however, did not include the Schiller–Naumann correction for drag, which could introduce some uncertainties. Zhang and Ahmadi (2000) investigated the particle deposition under effect of gravity. They found negligible effect of gravity direction for the fluid Reynolds number considered here ($Re_\tau = 180$). This result is in a clear contradiction with the recent findings of Marchioli et al. (2007) and Rousta et al. (2023) that show a significant effect of gravity direction on the deposition rate. This might trace back to the insufficient number of particles used in the work of Zhang and Ahmadi (2000) (about 8000 particles), which might have prevented accumulating reliable statistics. Additionally, they used the original Saffman lift force that clearly is not appropriate to study particle near-wall dynamics relevant to deposition.

Narayanan et al. (2003) studied particle deposition in an open channel and indicated that the dominant mechanism for small Stokes numbers is the "diffusional deposition" mechanism, i.e. long-time near-wall residence, and as the Stokes number increases the "free-flight deposition" mechanism (driven by turbophoresis), i.e. particles with large wall-normal velocities and short near-wall residence time, becomes stronger.

There are some reports on various modeling approaches to study particle deposition. Guha (2008) discussed Eulerian deposition models developed primarily based on the "free flight" concept. A detailed analysis of these models clearly demonstrates that they attempt to

describe the deposition process based solely on particle mass balance in the presence of particle concentration gradient (the Reynolds analogy), at best, which leads to a severe underestimation of the turbulence effects, such as turbophoresis on particle deposition which leads to severe inaccuracy as shown in Paes et al. (2015).

Soldati and Marchioli (2009) presented physical insights on particle entrapment and deposition and demonstrated the complex interactions of particles with coherent turbulent structures controlling the deposition process. Soltani and Ahmadi (1995) and Ounis et al. (1991) studied the role of these interactions in deposition of small particles, while Kaftori et al. (1995), Marchioli and Soldati (2002), Sardina et al. (2012) and Xiao et al. (2020) investigated large particles. They concluded that strong correlations between sweep events, i.e. high-speed fluid motion towards the wall, and flux of small particles towards the wall is the dominant cause for deposition, while ejection events, i.e. low-speed fluid motion towards the outer flow, contribute to transport of particles to the core of the channel.

It should be noted here that the studies mentioned before used a high fidelity framework, i.e. PP–DNS, to examine the particle transport and deposition in wall-bounded turbulent flows. However, their investigations were mostly focused on the effect of particle Stokes number on the transport and deposition. Additionally, most of them considered only the drag force on particle (Narayanan et al., 2003; Kuerten, 2006; Soldati and Marchioli, 2009; Sardina et al., 2012), while other forces such as lift and gravitational force (buoyancy) may alter the transport and deposition dynamics (Marchioli et al., 2007; Mortimer et al., 2019; Rousta et al., 2023).

Brandt and Coletti (2022) have recently also noted that gravity is required to be considered in most of the applications and the conclusions drawn from zero gravity studies should not be extrapolated to their practical settings. Furthermore, they suggested that Stokes number by itself may not contain enough information to describe all essential particle transport dynamics necessary to accurately capture the deposition dynamics.

Therefore, the current study aims to provide a more detailed and comprehensive understanding of the deposition process in turbulent wall–bounded flows. Towards this, we will demonstrate that different combinations of particle size (diameter) and properties (density) that result in an identical Stokes number present different deposition dynamics (rates). Specifically, with the assumption of dilute system and thus one-way coupling, several PP– DNSs have been conducted for turbulent channel flow at $Re_\tau = 180$ (defined in Section 3.1) to investigate the deposition dynamics for two Stokes Numbers ($St = 1$ and 10) that are results of different combinations of particle diameters and densities (See Table 1 for details). Moreover, as detailed in Table 1, for each combination, the effect of various forces on the deposition process is assessed. Again, we would like to note here that the primary goal of this study is to demonstrate the multi-dimensionality and complexity of the deposition process, i.e. the deposition rate cannot be described solely based on the Stokes number, consistent with the reporting of Brandt and Coletti (2022).

First, in Section 2 we explain the governing equations for the fluid phase and particle motion. Section 3 describes the computational domain, our setup for the simulations as well as the validation of our numerical simulations. Afterward, we discuss our results in Section 4 and conclude our work in Section 5.

2. Physical background

Here, we briefly explain the governing equations for a turbulent flow from DNS perspective and then the equation of motion for particles. We note that all the variables with + mark are written in dimensionless form based on the fluid kinematic viscosity (ν) and the friction velocity ($u_\tau = \sqrt{\left(\frac{\tau_w}{\rho}\right)}$), with ρ being the fluid density and τ_w wall shear stress, such that length is scaled with $l^+ = lu_\tau/\nu$, velocity with $u^+ = u/u_\tau$ and time with $t^+ = tu_\tau^2/\nu$.

2.1. Fluid equations of motion

For an incompressible, single-phase fluid flow, Continuity and Navier–Stokes equations in the dimensionless form (based on u_τ and h) are as follows:

$$\nabla \cdot \mathbf{u}^+ = 0 \tag{1}$$

$$\frac{\partial \mathbf{u}^+}{\partial t^+} + \mathbf{u}^+ \cdot \nabla \mathbf{u}^+ = \frac{1}{Re_\tau}\nabla^2 \mathbf{u}^+ - \nabla p^+ + \delta^+_{i,1}, \tag{2}$$

where $\mathbf{u}^+$ and p^+ are fluid velocity and kinematic pressure, respectively, and $\delta^+_{i,1}$ is a constant pressure gradient which drives the flow. The friction Reynolds number is computed as $Re_\tau = hu_\tau/\nu$ where h is the channel half width.

2.2. Particle tracking

Here, the particle trajectory is tracked individually. Therefore, the equation of motion for each particle is solved during the simulation. The Lagrangian equation of motion is written in the dimensionless form as follows:

$$\frac{d\mathbf{r}_p^+}{dt^+} = \mathbf{v}_p^+ \tag{3}$$

$$\frac{d\mathbf{v}_p^+}{dt^+} = \mathbf{a}_D^+ + \mathbf{a}_L^+ + \mathbf{a}_G^+ \tag{4}$$

where $\mathbf{r}_p^+$ shows the particle position, $\mathbf{v}_p^+$, $\mathbf{a}_D^+$, $\mathbf{a}_L^+$ and $\mathbf{a}_G^+$ are the particle velocity and accelerations due to drag, lift and gravity, respectively. We define each acceleration in terms of the particle properties and Stokes number. Particle's Stokes number is the time that takes the particle to reach equilibrium with its surroundings with respect to the characteristic time of flow and it is defined as

$$St = \frac{\tau_p}{\tau_f} \tag{5}$$

where

$$\tau_p = \frac{\rho_p d_p^2}{18\rho\nu} \tag{6}$$

and

$$\tau_f = \frac{\nu}{u_\tau^2}. \tag{7}$$

The drag and lift accelerations are resulted from interactions between particle and fluid flow. Here, drag acceleration with empirical correlation (Schiller and Naumann, 1935) for drag coefficient is given by

$$\mathbf{a}_D^+ = \frac{\mathbf{u}_f^+ - \mathbf{v}_p^+}{St}\left(1 + 0.15Re_p^{0.687}\right)C_{DW} \tag{8}$$

where $\mathbf{u}_f^+$ is the fluid velocity at the location of particle and particle Reynolds number is defined as $Re_p = |\mathbf{u}_f - \mathbf{v}_p|d_p/\nu$. C_{DW} is the modification to the drag due to the vicinity of the particle to a solid boundary. It has been pointed out that wall modifications might affect the deposition process (Dance and Maxey, 2003; Arcen et al., 2006; Molin et al., 2012), and since the primary purpose of our work is to determine a reliable deposition velocity, we include the wall corrections as well. The wall corrections were derived by Faxen (1923) and Maude (1965) for a particle moving parallel ($C_{DW\parallel}$) and normal ($C_{DW\perp}$) to the wall, respectively, as below

$$C_{DW\parallel} = \left[1 - \frac{9}{16}\left(\frac{d_p^+}{2l_p^+}\right) + \frac{1}{8}\left(\frac{d_p^+}{2l_p^+}\right)^3 - \frac{45}{256}\left(\frac{d_p^+}{2l_p^+}\right)^4 - \frac{1}{16}\left(\frac{d_p^+}{2l_p^+}\right)^5\right]^{-1} \tag{9}$$

$$C_{DW\perp} = 1 + \frac{9}{8}\left(\frac{d_p^+}{2l_p^+}\right) + \left(\frac{9}{8}\frac{d_p^+}{2l_p^+}\right)^2 \tag{10}$$

where l_p^+ is the dimensionless distance of particle to the nearest wall.

The widely used lift model is the Saffman lift (Saffman, 1965) which was extended for finite Reynolds numbers with a correction J_L proposed by Mei (1992), which is essentially a curve fit of the tabulated results from McLaughlin (1991). However, there is an additional lift when particle is in the vicinity of the wall ($a_{L\,W}^{+\prime}$). Therefore, the lift acceleration can be written as

$$\mathbf{a}_L^+ = 0.1714 J_L \frac{d_p^+ \left|\mathbf{u}_f^+ - \mathbf{v}_p^+\right|}{St} \sqrt{\boldsymbol{\omega}^+} \frac{\left(\mathbf{u}_f^+ - \mathbf{v}_p^+\right) \times \boldsymbol{\omega}^+}{\left|\mathbf{u}_f^+ - \mathbf{v}_p^+\right| |\boldsymbol{\omega}^+|} + a_{L\,W}^{+\prime} \tag{11}$$

where

$$J_L = 0.3\left(1 + \tanh\left[\frac{5}{2}\left(\log_{10}\varepsilon + 0.191\right)\right]\right)\left(\frac{2}{3} + \tanh\left(6\varepsilon - 1.92\right)\right) \tag{12}$$

$$\varepsilon = \frac{\sqrt{\boldsymbol{\omega}^+}}{\left|\mathbf{u}_f^+ - \mathbf{v}_p^+\right|} \tag{13}$$

and $a_{L\,W}^{+\prime}$ is the wall-induced lift acceleration. Here, the near wall lift acceleration is calculated according to Takemura and Magnaudet (2003), which is defined as

$$a_{L\,W}^{+\prime} = \frac{3}{4} \frac{1}{\frac{\rho_p}{\rho} d_p^+} V_{LW}^{+\,2} C_{LW} \tag{14}$$

$$C_{LW} = C_{LW0}\left(1 + 0.6 Re^{0.5}{}_{LW} - 0.55 Re^{0.08}{}_{LW}\right)^2 \left(\frac{1}{3}\frac{2l_p^+}{d_p^+}\right)^{-2\tanh\left(0.01 Re_{LW}\right)} \tag{15}$$

$$C_{LW0} = \begin{cases} \left[\frac{9}{8} + 5.78\times10^{-6} z^{*4.58}\right] \exp\left(-0.292 z^*\right) & for \quad z^* \le 10 \\ 8.94 (z^*)^{-2.09} & for \quad z^* > 10 \end{cases} \tag{16}$$

where $V_{LW} = \left(\left[u_{x,f} - v_{x,p}\right]^2 + \left[u_{y,f} - v_{y,p}\right]^2\right)^{0.5}$ is the relative velocity in the wall-parallel plane, $Re_{LW} = V_{LW} d_p / \nu$ is the Reynolds number based on the relative velocity and $z^* = z_p V_{LW}/\nu$ is the non-dimensional distance of particle from the wall. This wall correction is consistent with the corrections of Vasseur and Cox (1977), discussed in Ref. Arcen et al. (2006), for the settings considered here (Takemura and Magnaudet, 2003; Shi and Rzehak, 2020).

The gravitational acceleration in a vector form considering the Buoyancy effect is defined as follows:

$$\mathbf{a}_G^+ = \left(1 - \frac{1}{\frac{\rho_p}{\rho}}\right) \mathbf{g}^+ \tag{17}$$

where absolute magnitude of non-dimensional gravitational acceleration is $g^+ = g\nu/u_\tau^3 = 0.0546$.

2.2.1. Particle deposition

The deposition velocity is defined as the particle flow rate (J^+) on the wall normalized by the mean bulk density of particles (mass of particles per unit volume C_0)

$$u_d^+ = \frac{J^+}{C_0}. \tag{18}$$

The particle flux can be written as the number of particles depositing (N_{dep}) per unit area per unit time

$$J^+ = \frac{1}{L^+ W^+} \frac{\Delta N_{dep}}{\Delta t^+}, \tag{19}$$

and C_0 is written as the total number of particles per unit volume

$$C_0 = \frac{N_0}{L^+ W^+ H^+} \tag{20}$$

where L^+ and W^+ are dimensionless length and width of the domain, respectively, and H^+ is the height of the channel occupied by the particles. Therefore, one could calculate the deposition velocity by replacing Eqs. (19) and (20) into Eq. (18) with the following for the dimensionless deposition velocity:

$$u_d^+ = \frac{\Delta N_{dep} H^+}{N_0 \Delta t^+}. \tag{21}$$

3. Computational setup

In this section, we provide details on our PP–DNS framework, its validation, the computational domain and our test cases.

3.1. Carrier phase

The incompressible Navier–Stokes equations are solved with a second-order finite difference method on a structured Cartesian grid using a fast-Fourier transform based method integrated in time with a three-step Runge–Kutta scheme (RK3), called **CaNS** (Canonical Navier–Stokes) (Costa, 2018). The simulations are carried out for a turbulent vertical channel flow at $Re_\tau = 180$ with periodic boundaries in streamwise and spanwise directions and no-slip boundary condition in wall-normal. The flow is driven with a constant pressure gradient (see Eq. (2)). The size of the domain is $4\pi h \times 2\pi h \times 2h$ in streamwise, spanwise and wall-normal direction, respectively, where $h = 2$ cm, and the domain is discretized with $512 \times 256 \times 144$ nodes, corresponding to $\Delta x^+ = 4.4$, $\Delta y^+ = 4.4$ and $\Delta z^+ = 0.3 \to 5$. The fluid is considered to be air with the viscosity of $\nu = 1.57 \times 10^{-5}$ m^2/s and the time step is $\Delta t^+ = 0.11$. In Fig. 2(b) a simple schematic of the computational domain is presented.

3.2. Particle motion

The CaNS code is coupled to a Lagrangian particle tracking (LPT) solver in a one-way fashion, i.e. the effects of particle motion on fluid phase is ignored with the assumption of a dilute system. The particle equations of motion are solved using a second-order Runge–Kutta scheme with the same time step as the fluid phase. Also, the fluid information, i.e. fluid velocity and vorticity, at each particle's position is computed with trilinear interpolation. It is mentioned by Johnson et al. (2020) and also Sardina et al. (2012) that this second-order interpolation method is accurate enough for PP–DNS and there is no need to increase the accuracy of the interpolation. For each set, 10^5 particles are randomly injected into the domain and assigned with the interpolated fluid velocity at the particle position. The periodic boundary conditions in streamwise and spanwise directions are applied for the particles as well such that when a particle leaves the domain, it re-enters the domain from the opposite side. The wall is considered as a trap wall, which means that when distance of a particle to the wall gets less than the particle radius, the particle is deposited and removed from the domain. Yet to keep the total number of the particles constant during the simulation, one particle is added to the domain in a random location. The trap wall is chosen to resemble sticky systems.

3.3. Validation

We validate our PP–DNS framework against the data provided by Marchioli et al. (2008). In their international collaborative work, they have provided 5 datasets from 5 different groups. Here, we have only used the data from UUD group, i.e. C. Marchioli and A. Soldati. Shear Reynolds number in this benchmark case is $Re_\tau = 150$ and we choose the smallest and largest Stokes numbers for the validation. We obtain the statistics similary to the reference after the particles reach a statistically developed condition (Marchioli et al., 2008) (see Section 4). Fig. 3 presents the mean streamwise velocity and Fig. 4 shows RMS of velocity in streamwise and wall-normal direction. Overall, our results show a good agreement with the reference data.

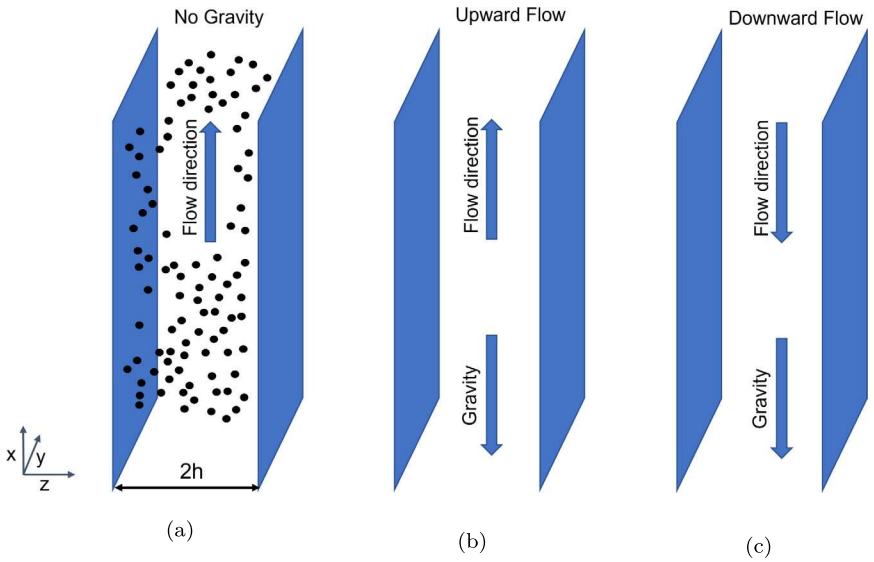

Fig. 2. A schematic of the computational domain for a channel at (a) zero gravity, (b) with flow in the opposite direction of gravity and (c) flow in the same direction as gravity.

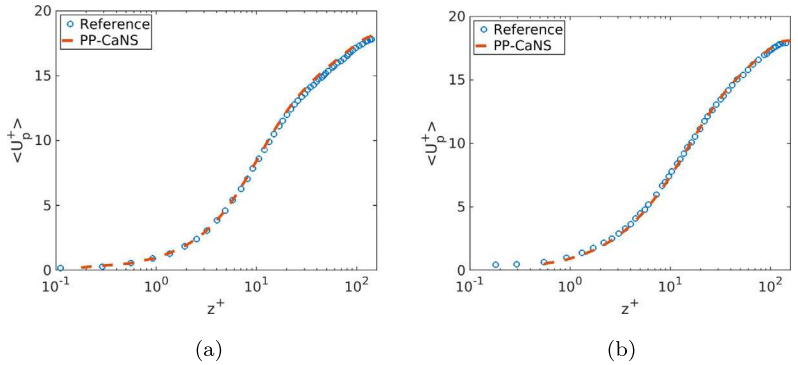

Fig. 3. Mean particle streamwise velocity profiles for (a) $St = 1$ and (b) $St = 25$ along the wall. Our results show a very good agreement with reference data from Marchioli et al. (2008).

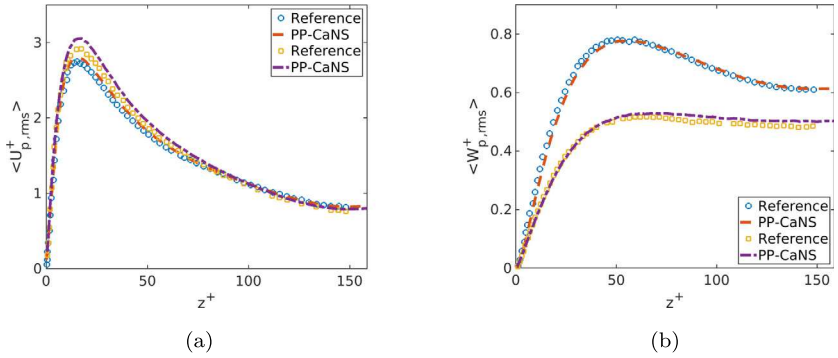

Fig. 4. RMS of the particle velocity in (a) streamwise and (b) wall-normal direction along the wall. ○ and □ show the reference data for $St = 1$ and $St = 25$, respectively, from Marchioli et al. (2008) and dashed line and point-dash line represent our simulation results for $St = 1$ and $St = 25$.

3.4. Test cases

The main purpose of this work is to study the deposition process in wall-bounded flows. As discussed before, deposition is a multi-dimensional process (depends on several parameters) and cannot be described solely based on the Stokes number. More specifically, the deposition rate is a function of particle diameter, particle density, considered forces as well as Kolmogorov length scale associated with the fluid phase for a given configuration and Reynolds number. The main intention of the current effort is to demonstrate such complex dynamics. Therefore, five sets of simulations have been designed for two different Stokes numbers. In particular, different particle diameters and densities have been used to create the same Stokes numbers. A summary of simulation setups is given in Table 1. It is worth noting that majority of previous investigations on particle dispersion and deposition in a one-way coupled fashion are based on obtaining various Stokes numbers, either with constant particle density and changing particle diameter (Marchioli et al., 2008) or vise versa (Mortimer et al.,

Table 1
A summary of simulation cases and particle properties. A schematic of upward case is shown in Fig. 2(c) and for downward in Fig. 2(d).

St	d_p [μm]	d^+_p	$\frac{\rho_p}{\rho}$	Accelerations	Case
1	4.8	0.043	9500	Drag	case(a-1)
				Drag+Lift	case(b-1)
				Drag+Lift+Gravity (upward)	case(c-1)
				Drag+Lift+Gravity (downward)	case(d-1)
	15.3	0.138	950	Drag	case(a-2)
				Drag+Lift	case(b-2)
				Drag+Lift+Gravity (upward)	case(c-2)
				Drag+Lift+Gravity (downward)	case(d-2)
	48	0.43	90	Drag	case(a-3)
				Drag+Lift	case(b-3)
10	15.3	0.138	9500	Drag	case(a-4)
				Drag+Lift	case(b-4)
				Drag+Lift+Gravity (upward)	case(c-4)
				Drag+Lift+Gravity (downward)	case(d-4)
	48	0.43	950	Drag	case(a-5)
				Drag+Lift	case(b-5)
				Drag+Lift+Gravity (upward)	case(c-5)
				Drag+Lift+Gravity (downward)	case(d-5)

2019; Johnson et al., 2020). We will assess validity of such an approach in this study.

The baseline simulation for each particle size includes the drag acceleration only. Effects of lift and gravity on particle dispersion and deposition will be studied based on particle size and density, in contrast to previous studies that such effects were analyzed solely based on the Stokes number (Marchioli et al., 2007; Rousta et al., 2023). Additionally, in our study two flow directions were considered (cf. Fig. 2) to assess the effects of gravity when acting as accelerator as well as decelerator. Lift and gravity were added in a step-by-step fashion. It should be noted that the effect of gravity is considered for Aerosol cases (i.e. $\rho_p/\rho > 1000$), therefore, for the case(*-3) with $\rho_p/\rho = 100$ only effect of lift is studied. The simulations carried out with only the drag force are referred to as group a, the simulations with drag and lift group b, drag, lift and gravity in an upward flow group c and drag, lift and gravity in a downward flow group d, respectively (see Table 1).

4. Results

In this section, we explain the results in the order of the added accelerations in the simulations. As mentioned, the baseline simulations include solely the drag acceleration, and lift and gravity are included step by step (cf. Fig. 2 and Table 1).

To compute the statistics, the domain in wall-normal direction is divided into $N_s = 193$ non-uniform slabs and particle statistics are gathered for each slab and then time-averaged quantities are computed. Thickness of each slab is computed by hyperbolic-tangent binning (Marchioli et al., 2008) with stretching factor of $\gamma = 1.7$:

$$\Delta z^+(s) = \frac{Re_\tau}{\tanh\gamma}\left[\tanh\left(\gamma\frac{s}{N_s}\right) - \tanh\left(\gamma\frac{s-1}{N_s}\right)\right] \quad (22)$$

The total time of simulations is $t^+ = 45{,}000$ and to ensure that the particles have statistically reached a steady state, we start collecting the statistics after the mean particle concentration near the wall reaches an approximately constant value. Fig. 5 displays the instantaneous number of particles in the first slab alongside the wall. Smaller Stokes number and smaller particles (Fig. 5(a)) take longer times to get to the fully developed state. As the Stokes number and particle size increase, the necessary time to get to the statistically steady state becomes shorter, as illustrated in Fig. 5(b). Additionally, as it appears in the plots when lift and gravity are added the particles reach a developed state in a shorter time (we discuss the effect of each force in the following sections). For the results shown in this work, we have calculated the statistics after $t^+ = 25{,}000$ to ensure statistically steadiness for all the cases.

In simulations with only drag, case(a-*), since the relaxation times for particles with the same Stokes number are similar, the drag accelerations are also analogous, however particle concentration profiles are different (Figs. 7(a) and 7(c)). This difference could be due to the particle diameter. In other words, even if two particles with different sizes have the same trajectory, they have different contact points with the wall (particle radius). Therefore, particles could have different concentrations and also deposition rates (cf. Table 2) at the same Stokes number. In what follows the relationships between lift and gravity effects with particle characteristics will be studied. This also can be visualized with Voronoi tessellation method (Monchaux et al., 2010; Fong et al., 2019). In the Voronoi method the domain is divided into cells, such that each cell represent an individual particle with its instantaneous local concentration. Therefore, this method is used to identify regions where particle clustering occurs. The threshold necessary for this method is obtained from a Voronoi tessellation of a randomly distributed particles. Fig. 6 shows the Voronoi diagram at the mid-plane (x-z) for cases (a-4) and (a-5) ($St = 10$, $d_p = 15.3$ and 48 μm). The cell areas are colored with respect to a Voronoi analysis of an initial random particle distribution. It can be observed that the larger particles (48 μm) show more clustering overall and in particular, around the buffer layer and therefore higher deposition rate. This result clearly demonstrate that particle clustering also depends on particle size in addition to the Stokes number.

4.1. Analysis of the correlation between lift effects and particle characteristics

To compare dispersion of particles with different characteristics when lift is included, the mean concentration profiles in wall-normal direction are demonstrated in Fig. 7. As one could observe, same Stokes numbers with different particle sizes have different particle concentrations near the wall. Figs. 7(a) and 7(b), indicate that for $St = 1$ and $d_p = 4.8$ and 15.3 μm, lift acceleration has a negligible effect on the magnitude of near-wall particle concentration. However, there is a noticeable change for the largest particle $d_p = 48$ μm likely due to the dependency of lift on the particle diameter. In contrast, the effect of lift is clearer for larger Stokes number (Figs. 7(c) and 7(d)), which shows a decrease in particle near-wall concentration. However, different particle sizes have different concentrations and consequently different deposition rates. Overall, one could conclude that including the lift acceleration in the particle motion, could lead to a reduction of

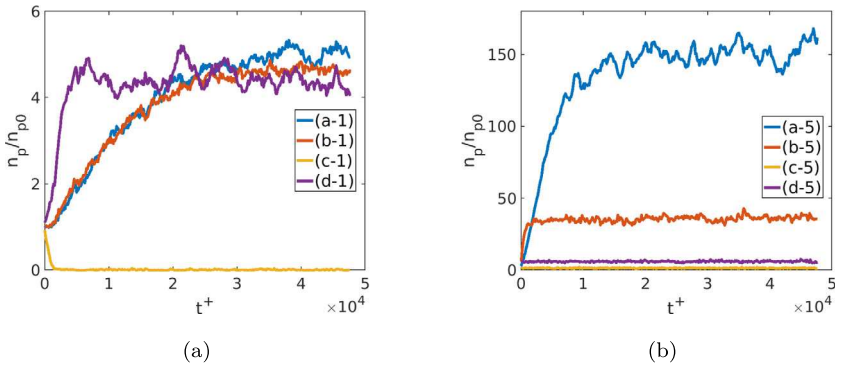

Fig. 5. Instantaneous number of particles near wall for (a) $St = 1$ (case (*-1)) and (b) $St = 10$ (case(*-5)). The time duration to get to a fully developed state reduces with the increase of particle size and Stokes number as well as included accelerations.

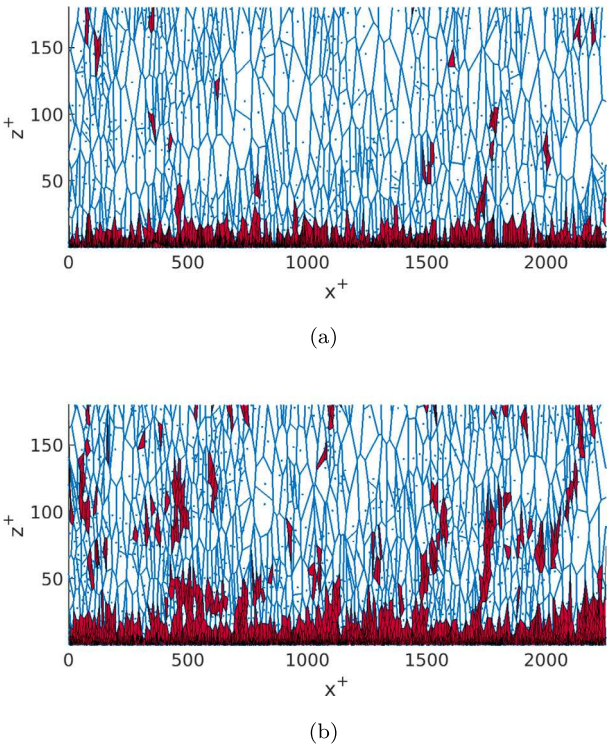

Fig. 6. Instantaneous Voronoi diagram for (a) case(a-4) and (b) case(a-5) in the mid-plane. There are more clusters in the wall region for the larger particles and therefore the deposition is higher for the larger particle even at the same Stokes number.

particle near-wall concentration at high density ratios, a situation that resemble Aerosol dynamics with $\rho_p/\rho > 1000$. This decrease in concentration is related to the significant increase of the deposition velocity (cf. Table 2). The reason for this change could be comprehended from the profile of accelerations in Fig. 8.

The results presented in Fig. 8 clearly demonstrate that for the same Stokes number, the acceleration due to the drag is identical. This behavior of drag acceleration is consistent with its formulation, i.e. drag acceleration is solely a function of the Stokes number, i.e. different particle sizes experience the same drag acceleration. Also the drag acceleration does not show any substantial sensitivity when lift is included. Therefore, only the acceleration due to drag for cases (b-*) is shown in Figs. 8(a) and 8(b).

On the other hand, the lift acceleration is different for all the cases shown in Figs. 8(c) and 8(d) because the lift acceleration is dependent on the particle diameter as well as the Stokes number (Eq. (11)). As mentioned in previous studies (Marchioli and Soldati, 2002; Soldati and Marchioli, 2009; Rousta et al., 2023), there are two mechanisms causing the deposition; (i) diffusion for particles residing near the wall for a long time, and (ii) impaction due to turbophoresis. For the smaller Stokes number ($St = 1$) lift (Fig. 8(c)) has small but different impacts on the near wall concentration. For small particles, i.e. $d_p = 4.8$ μm and 15.3 μm (cases (b-1) and (b-2) in Figs. 7(a) and 7(b)), it causes a decrease in mean particle wall-normal velocity, which results in slight reduction in deposition rate. However, considering the largest particle $d_p = 48$ μm (case (b-3) in Figs. 7(a) and 7(b)), the accelerations due to lift and drag are almost of the same order (case (b-3) in Figs. 8(a) and 8(c)), which helps the particles to get deposited with impaction. For $St = 10$ with $d_p = 15.3$ μm and 48 μm, the lift behavior becomes more complex (cases (b-4) and (b-5) in Fig. 8(d)). The positive lift near the wall region ($1 < z^+ < 5$) pushes the particles towards the buffer layer and the negative lift in the outer region brings the particles also in the buffer layer ($5 < z^+ < 30$), which increases the clustering of the particles in that region and consequently, the rate of the deposition due to turbophoresis. The increase in the deposition velocity ultimately leads to a reduction of near-wall concentration mainly due to the trap

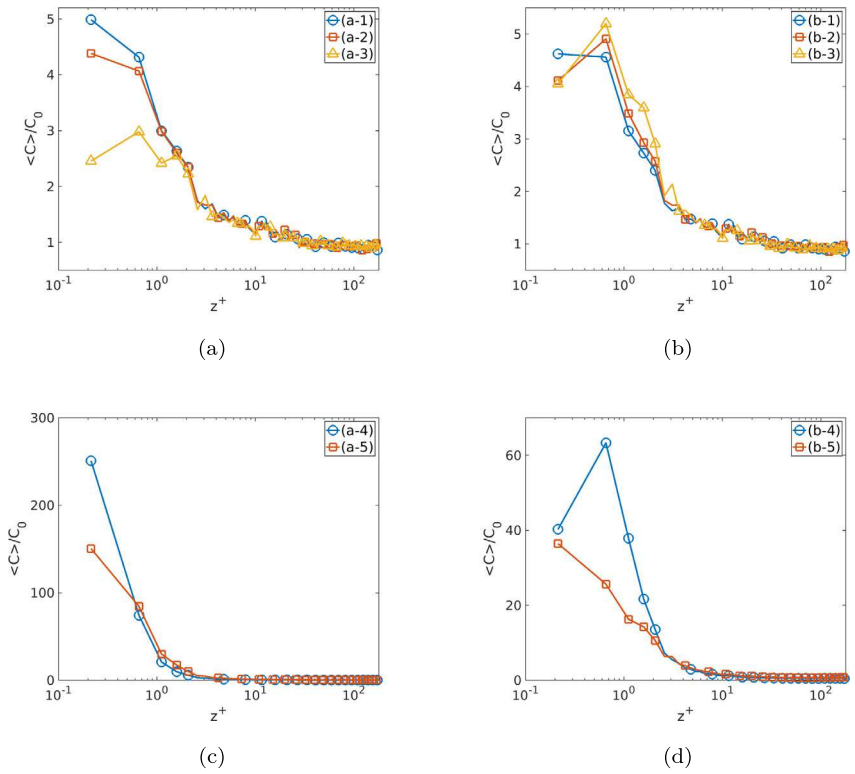

Fig. 7. Mean concentration profile with only drag considered for (a) $St = 1$ and (c) $St = 10$ and with drag and lift for (b) $St = 1$ and (d) $St = 10$. Lift increases the deposition for large particles/Stokes numbers which results in lower concentration near wall due to trap wall boundary condition.

wall boundary condition (cases (b-4) and (b-5) in Fig. 7). Therefore, one could see that for the cases with the same Stokes numbers, when particle size increases, the magnitude of lift also increases and thus, impacts the deposition velocity noticeably.

Supporting previous arguments, the time-averaged velocity profiles in streamwise direction are shown in Fig. 9. It should be noted that due to similar results for each Stokes we present the velocity statistics for only one particle size (cases (*-2) and (*-5)). For small Stokes number, there is no significant changes in velocity magnitude when the lift is added in the simulations. For the larger Stokes number, the particle velocity is slightly larger than the fluid velocity in the viscous sublayer, hence the positive lift direction (away from the wall), and smaller than the fluid velocity in the buffer layer and therefore, the lift is negative (towards the wall).

Furthermore, the particle velocity variances in streamwise and wall-normal directions do not show considerable changes as demonstrated in Fig. 10. Thus, our results here indicate that the acceleration due to lift might have small effects on particle velocity statistics but might change the deposition rate considerably.

It has been concluded in previous studies (Marchioli et al., 2007) that lift reduces the deposition for small Stokes numbers and increases the deposition velocity for large Stokes numbers. However, our results show that Stokes number is not the only determining parameter and other parameters such as particle size and density need to be considered to have a comprehensive picture on particle dynamics and deposition ($St = 1$ and $d_p = 48$ μm contracts the conclusion). This reason for this difference is explained in Section 4.3.

Finally, it is worth noting here that for particle sizes considered here, the particle velocity statistics (first order and second order) both reach a finite value at the contact point with the wall (unlike the fluid velocity variance that becomes zero at the wall). However, the particle velocity fluctuations appear to be much stronger than particle mean velocity when approaching the wall. This may suggest that for particles in the diffusion-impaction regime, the velocity variance is controlling the deposition process.

4.2. *Analysis of the correlation between lift and gravity effects and particle characteristics*

When studying the the connection between gravity and particle characteristics, we have considered two directions for flow; (i) upward flow i.e. opposite direction of gravity (Fig. 2(c)) and downward flow, same direction as gravity (Fig. 2(d)). Mean concentration profiles for all cases with gravity are shown in Fig. 11. First, we discuss the results for upward flow demonstrated in (Figs. 11(a) and 11(c)). The concentrations near the wall in the upward cases decrease in comparison to the cases with no gravity (cf. Fig. 7). When $St = 1$ is considered, drag does not experience any significant change in wall-normal direction (cases (c-1) and (c-2) in Fig. 12(a)), but gravity interacts with lift strongly and alters the particle dynamics, particularly close to the wall (cases (c-1) and (c-2) in Fig. 12(c)). As a result of this, particles move away from the wall because of the positive lift acceleration, which prevents the particles to accumulate in the wall region. Therefore, the concentration near the wall is reduced and consequently no deposition occurrs. Considering $St = 10$, gravity alters near-wall behavior of both drag and lift (cases (c-4) and (c-5) in Figs. 12(b) and 12(d)), which results in decrease of concentration and ultimately changes in the deposition rate.

In the downward cases, for the small Stokes number, the number of particles near the wall increases, and as a result, particles get deposited at a higher rate (Fig. 11(b)). The negative lift acceleration (cases (d-1) and (d-2) in Fig. 12(c)), which moves the particles towards the wall, is due to the change in stream-wise velocity with gravity. Considering the small particle ($d_p = 4.8$ μm) the drag acceleration does not change, but for the larger particle ($d_p = 15.3$ μm) there is a slight increase in drag (cases (d-1) and (d-2) in Fig. 12(a)).

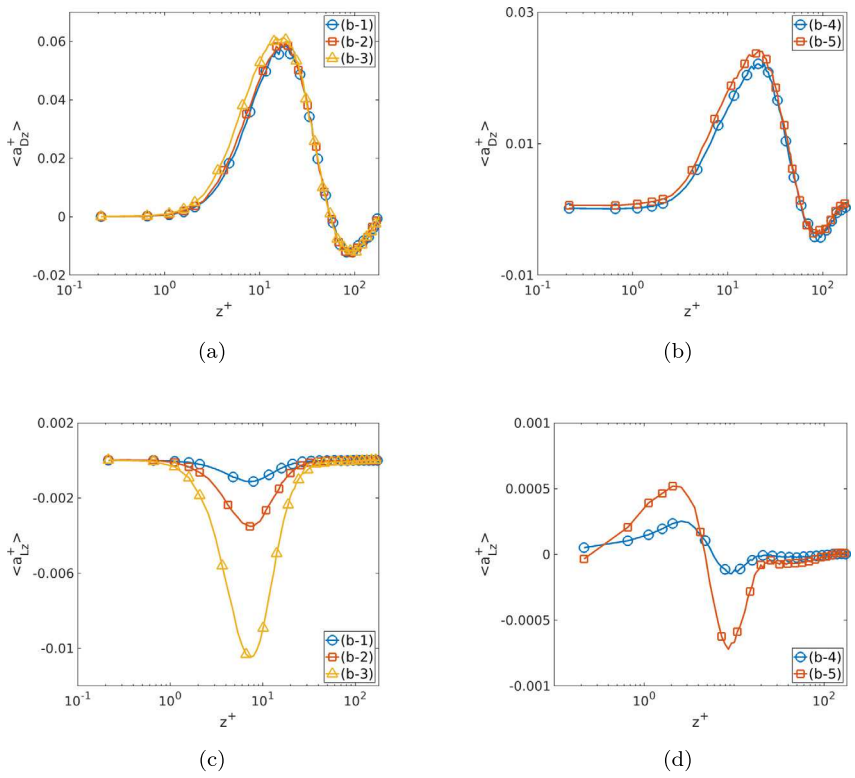

Fig. 8. Mean wall-normal acceleration due to drag for (a) $St = 1$ and (b) $St = 10$ and due to lift for (c) $St = 1$ and (d) $St = 10$ along the wall. While the drag acceleration is only dependent on Stokes number, the lift acceleration is a function of Stokes as well as dimensionless particle diameter. Therefore, different cases show different lift accelerations. The drag profiles for the cases without lift are qualitatively similar, and they are not shown here.

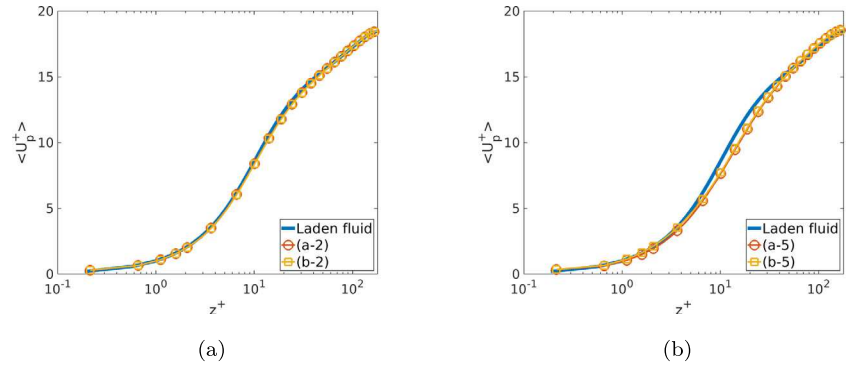

Fig. 9. Mean streamwise velocity profile for (a) $St = 1$ and (b) $St = 10$. Lift effect on mean velocity is very small. The profiles for other particle sizes with the same Stokes number are almost similar. Therefore they are not shown here.

Regarding the larger Stokes number, the concentration is reduced in comparison to the case with no gravity (Fig. 11(d)). The gravitational acceleration changes the profiles of drag (cases (d-4) and (d-5) in Fig. 12(b)) and lift (cases (d-4) and (d-5) in Fig. 12(d)) considerably in the downward case. The negative lift pushes the particles towards the wall and strengthens the deposition, and therefore increases the deposition velocity. We note again that low near-wall concentration in the downward cases is related to high rate of deposition since the particles are removed from the computational domain when deposited. Therefore, the lower concentration for the larger particle ($d_p = 48$ μm) is due to the higher lift and consequently higher deposition rate. The same pattern is observed in Ref. Rousta et al. (2023) with trap wall boundary condition.

In general, even though the drag acceleration is only dependent on the Stokes number, lift and gravity interact differently with drag for different particle characteristics and different modifications to drag acceleration occurs, even at the same Stokes number. Additionally, since the lift acceleration is dependent on Stokes number and particle size, each case shows a different lift acceleration in Figs. 12(c) and 12(d). It is worth noting that for heavy particles (aerosol) magnitude of lift acceleration increases as particles become larger, while the opposite trend is observed for light particles (bubbles) (Molin et al., 2012).

Supporting previous arguments, when the gravity is added in the simulations, the particle streamwise velocity changes (cf. Fig. 13), which causes changes in wall-normal lift and consequently drag accelerations. However, for $St = 1$, such changes are not significant due to the small relaxation time (Figs. 13(a), 14(a) and 14(c)). In contrast, for $St = 10$, one could observe that the streamwise velocity in the upward case is noticeably lower than the fluid velocity in the buffer layer (case (c-5) in Fig. 13(b)) and thus, the lift direction is moving the particles away from the wall (case (c-5) in Fig. 12(d)). On the other hand, for the downward flow case, the particle velocity in the streamwise direction

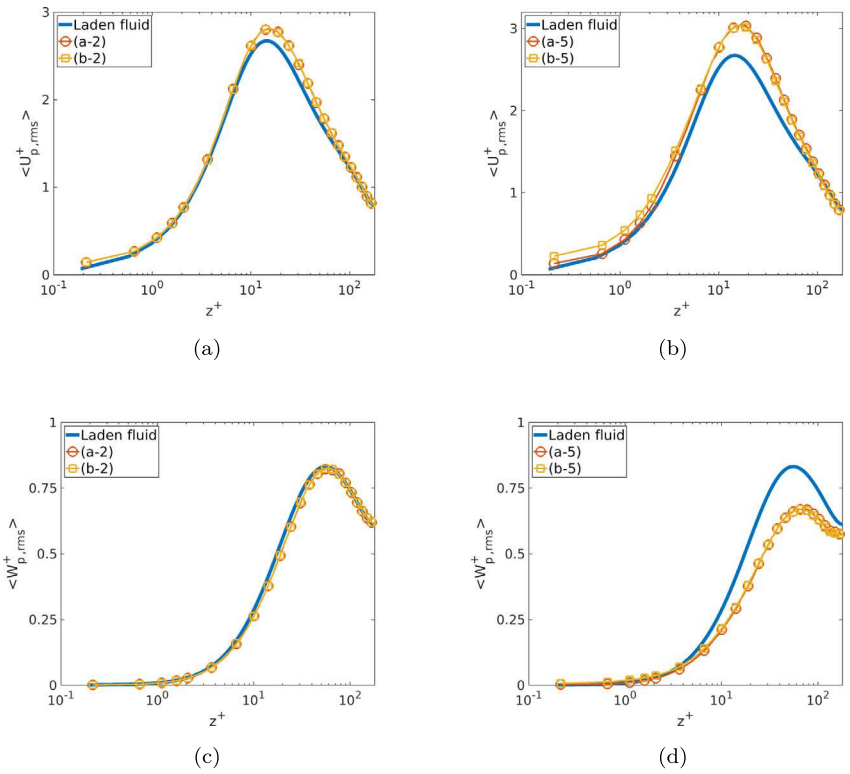

Fig. 10. RMS of the particle velocity in streamwise direction for (a) $St = 1$ and (b) $St = 10$ and wall-normal for (c) $St = 1$ and (d) $St = 10$ along the wall. For more explanation refer to Fig. 9.

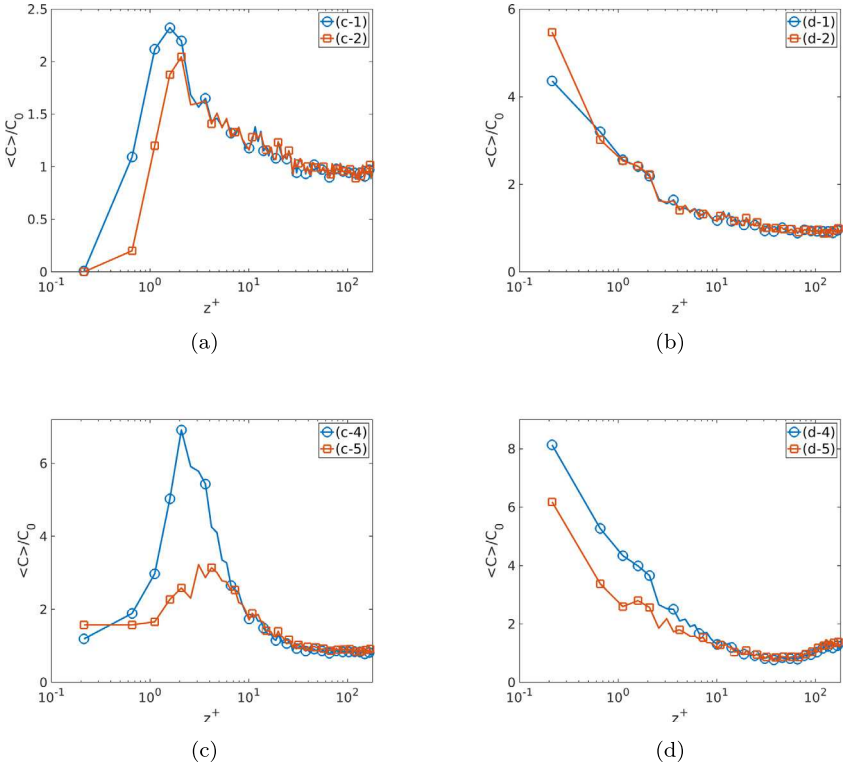

Fig. 11. Mean concentration profile with upward flow for (a) $St = 1$ and (c) $St = 10$ and downward flow for (b) $St = 1$ and (d) $St = 10$. In the upward flow particles are pushed away from the wall whereas in the downward flow particles are moved towards the wall.

is higher than the fluid velocity (case (d-5) in Fig. 13(b)) and the lift force pushes the particles towards the wall (case (d-5) in Fig. 12(d)) and therefore we observe a higher deposition velocity. Note that since the velocity statistics were almost similar for different particle sizes with the same Stokes number, only one of the cases is shown, i.e. case 2 and 5 in Figs. 13 and 14. Also, the RMS profiles are intensified for $St = 10$

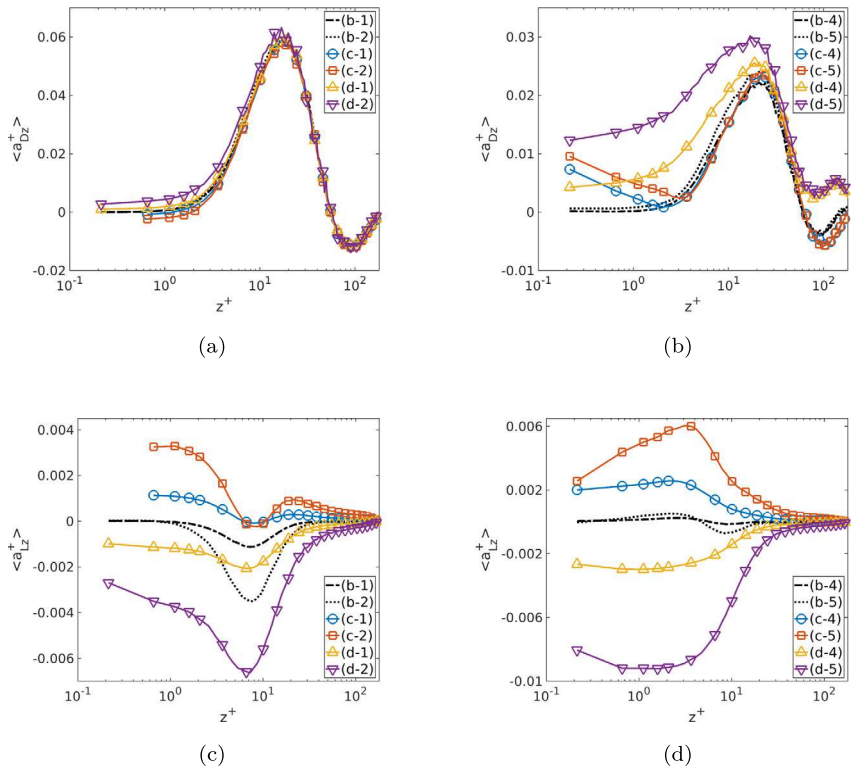

Fig. 12. Mean wall-normal acceleration due to drag for (a) $St = 1$ and (b) $St = 10$ and due to lift for (c) $St = 1$ and (d) $St = 10$ for upward and downward flow. The gravitational acceleration interact differently with drag and lift.

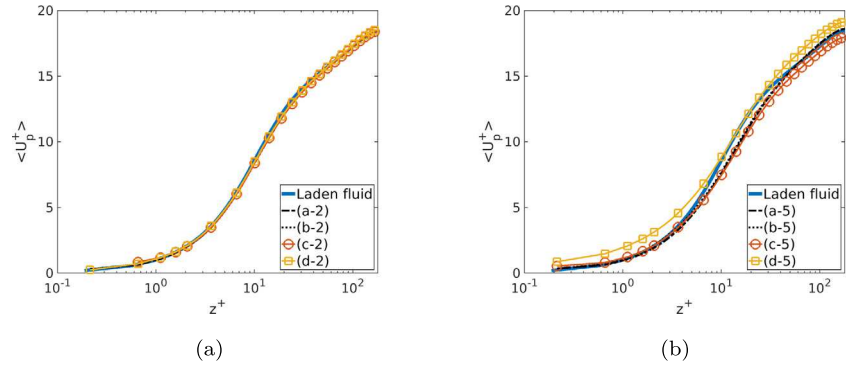

Fig. 13. Mean streamwise velocity profile for (a) $St = 1$ and (b) $St = 10$. Gravity affects the particle stream-wise velocity and its impact increases for the large Stokes number. The profiles for the other particle sizes are almost the same. Therefore they are not shown here.

(Figs. 14(b) and 14(d)), since the magnitudes of drag and lift change due to the effect of gravity.

Overall, we may conclude that not only Stokes number but also particle properties as well as the direction of the flow are important in the deposition investigations. Therefore, as mentioned recently (Brandt and Coletti, 2022), effect of gravity is important in particle deposition, and thus results obtained for zero-gravity cannot be extrapolated to non-zero gravity cases, even for small particles.

4.3. Deposition velocity

Table 2 presents the deposition velocity (rate) for each case including different acceleration mechanisms. For small Stokes numbers and small particles ($d_p = 4.8$ and 15.3 μm) the addition of lift reduces the deposition rate or in other words, decreases the number of particles with velocities towards the wall while an opposite effect is observed for $d_p = 48$ μm. This contrast can be explained by looking at the lift acceleration very close to the wall, i.e. where deposition occurs ($O(d_p^+)$). As mentioned before, lift is a function of Stokes number as well as particle diameter (Eq. (11)), and therefore, its characteristics vary for particles with different sizes, even at the same Stokes number. As pointed by McLaughlin (1989), wall-normal lift might not show any virtual effect outside the viscous sublayer region and beyond on particle statistics. However, even its small magnitude in the deposition region has a strong effect on particle deposition, i.e. exactly in a region that the wall-normal fluid velocity is negligible, even a small amount of lift can change the deposition rate. Therefore, considering $St = 1$, very close to the wall (deposition region) a positive lift decreases the deposition rate for small particles and a negative lift increases the deposition for the largest particle. Considering $St = 10$, lift works always in favor of the deposition process and increases the deposition velocity by pushing the particles towards the buffer layer and intensifying the deposition via impaction (turbophoresis). Considering the largest particle at this Stokes number, $d_p = 48$ μm, there is an additional effect coming from a negative lift very close to the wall, which in conjunction with

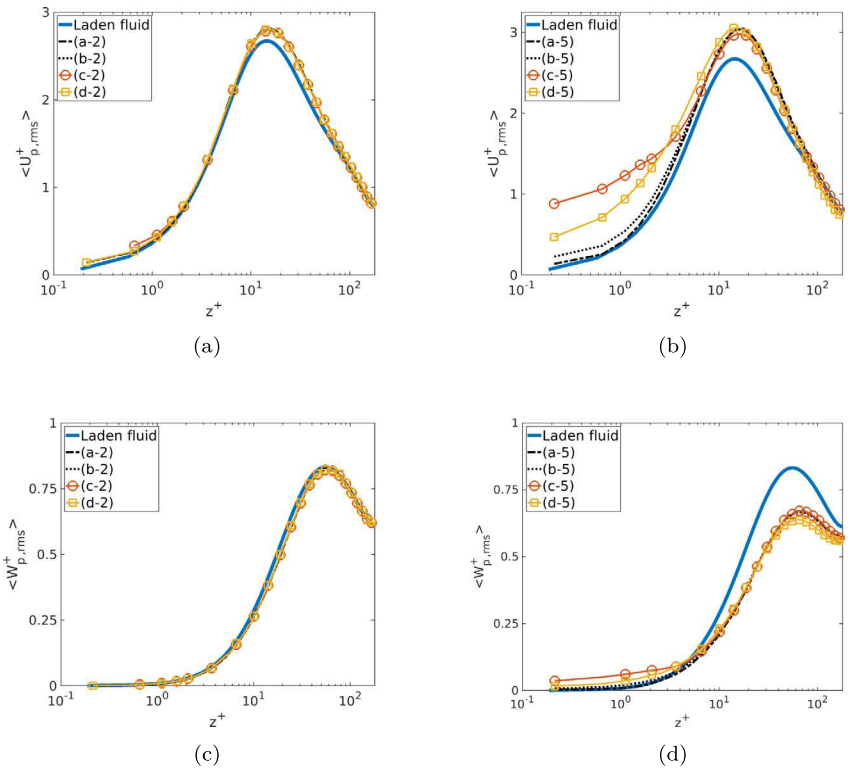

Fig. 14. RMS of the particle velocity in streamwise direction for (a) $St = 1$ and (b) $St = 10$ and wall-normal for (c) $St = 1$ and (d) $St = 10$ along the wall. For more explanation refer to Fig. 13.

Table 2
Calculated deposition velocity for all the cases.

Case	u^+_d	Case	u^+_d
(a-1)	2.2×10^{-5}	(b-1)	1.7×10^{-5}
(a-2)	4.7×10^{-5}	(b-2)	3.1×10^{-5}
(a-3)	1.2×10^{-4}	(b-3)	1.7×10^{-4}
(a-4)	0.012	(b-4)	0.024
(a-5)	0.017	(b-5)	0.049
(c-1)	0.	(d-1)	2.4×10^{-3}
(c-2)	0.	(d-2)	6.3×10^{-3}
(c-4)	0.034	(d-4)	0.123
(c-5)	0.033	(d-5)	0.153

turbophoresis further increases the deposition (see Fig. 8(d)-case (b-5) for negative lift very close to wall).

Additionally, as explained, the gravitational acceleration affects the particle streamwise velocity, which alters the lift in wall-normal direction and thus, particle wall-normal velocity and the deposition rate. However, considering $St = 10$, for the smaller particle, $d_p = 15.3$ μm, gravity increases the deposition due to higher lift and increasing the deposition via impaction, but it decreases the deposition velocity for the larger particle, $d_p = 48$ μm. This difference is thought to be due to the effect of gravity which eliminates the negative lift in the deposition region (see the explanation above).

To support our findings, we display the particle mean wall-normal velocity for case 5 (i.e. $St = 10$ and $d_p = 50$ μm) in Fig. 15. As explained, the change in wall-normal velocity statistics causes the change in deposition velocity. One could notice that the inclusion of lift (case (b-5)) increases the mean wall-normal velocity and consequently the deposition rate. For the upward case (c-5), despite the higher velocity near the wall in comparison to case (b-5), the wall-normal velocity in the buffer layer is lower, suggesting that fewer particles go towards the wall and get deposited by impaction. For the downward case (d-5), magnitude of the wall-normal velocity is much higher than the

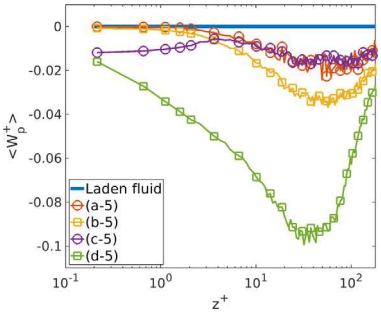

Fig. 15. Mean wall-normal velocity profile for $St = 10$ with $d_p = 50$ μm. The wall-normal velocity changes when different accelerations are considered and consequently changes the deposition rate.

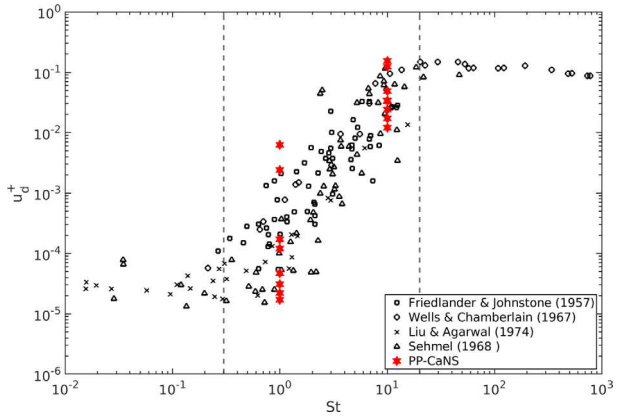

Fig. 16. Particle deposition velocity for different sets of studies. Our results fall in the accepted range. Experimental data are taken from Young and Leeming (1997).

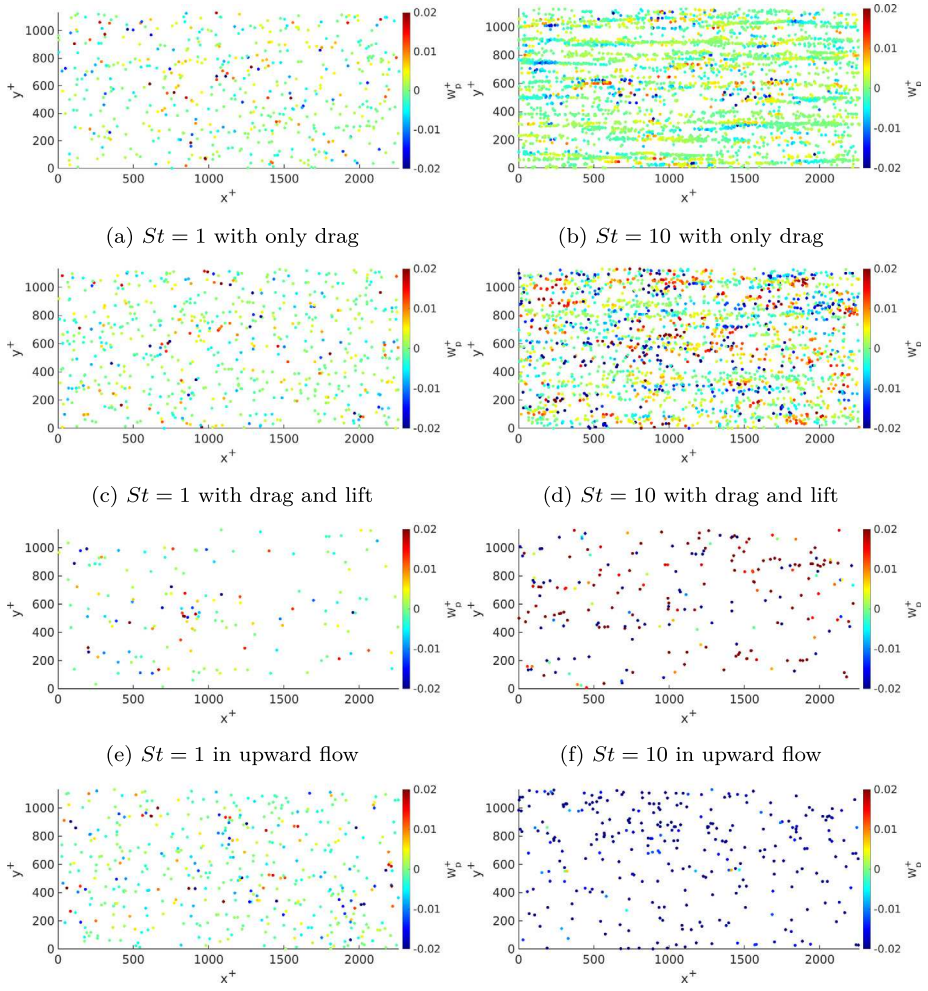

Fig. 17. Instantaneous particle distribution for case (a) (a-2), (b) (a-5), (c) (b-2), (d) (b-5), (e) (c-2), (f) (c-5), (g) (d-2) and (h) (d-5) in (x-y) plane with $z^+ = 1$ at $t^+ = 40000$. The gravity changes the dynamics of particles near the wall considerably for the larger Stokes number.

other cases which results in one order of magnitude larger deposition velocity.

Comparing our results with the available experimental data in Fig. 16, the deposition velocities for all the cases obtained here fall within the range of experiments. It can be observed that considering different combinations of material properties and/or different combinations of accelerations for the same Stokes number leads to different results. Therefore, the results presented here confirm the multi-dimensionality and complexity of the deposition process, that is deposition dynamics are dependent on particle characteristics as well as fluid phase properties and thus, cannot be described solely based on the Stokes number.

4.4. Particle near-wall dynamics

To have a qualitative visualization of near-wall particle segregation, we show snapshots of particle distribution at $z^+ = 1$ in Fig. 17. For smaller Stokes ($St = 1$), the particle distribution for all the cases demonstrate almost homogeneous distributions and including lift and gravity does not alter their location within the low-speed streaks, and only the number of particles reaching the deposition region changes (Figs. 17(a),17(c),17(e) and 17(g)). For larger Stokes ($St = 10$), we can observe the particle segregation in the regions with low-speed streaks (Fig. 17(b)). Including lift has a small effect on their distribution and a weak segregation can still be detected (Fig. 17(d)). However, including gravity in either direction disturbs their distribution and no specific pattern is observed (Figs. 17(f) and 17(h)). The same dynamics can be seen for case (*-1) and case (*-4) (not shown here).

In order to have a more quantitative comparison, we compare probability density function (PDF) of particle wall-normal velocity and slip velocity magnitude ($V_{slip} = |\mathbf{u}_f - \mathbf{v}_p|$) in Figs. 18 and 19, respectively. We show the PDFs for case(*-2) and case (*-5) in four separated regions; (1) deposition region ($z^+ \sim O(d_p^+)$), (2) Viscous sublayer ($O(d_p^+) < z^+ < 5$), (3) Buffer layer ($5 < z^+ < 30$) and (4) Outer region ($30 < z^+ < 180$). In the deposition region (Figs. 18(a) and 18(b)), the shift in particle wall-normal velocity is apparent, which changes the deposition rate. In the viscous sublayer, for the smaller Stokes number (Fig. 18(c)), particles reach an almost symmetric distribution, which shows that some particle move towards the wall and some move away from it. For the larger Stokes number (Fig. 18(d)), there is still an asymmetry distribution, which shows their tendency away from the wall, case (c-5), or towards the wall (d-5). For both Stokes numbers, particles have a homogeneous distribution towards the centerline and their PDFs are almost similar in the bulk flow region. As mentioned before, the reason in change of particle wall-normal velocity and consequently deposition rate is the lift acceleration, which is a function of particle diameter and Stokes number as well as slip velocity, which also significantly gets affected by gravity. The change in slip velocity can be seen in Fig. 19 for different regions. Including gravity changes the streamwise velocity that results in a higher slip velocity for both upward

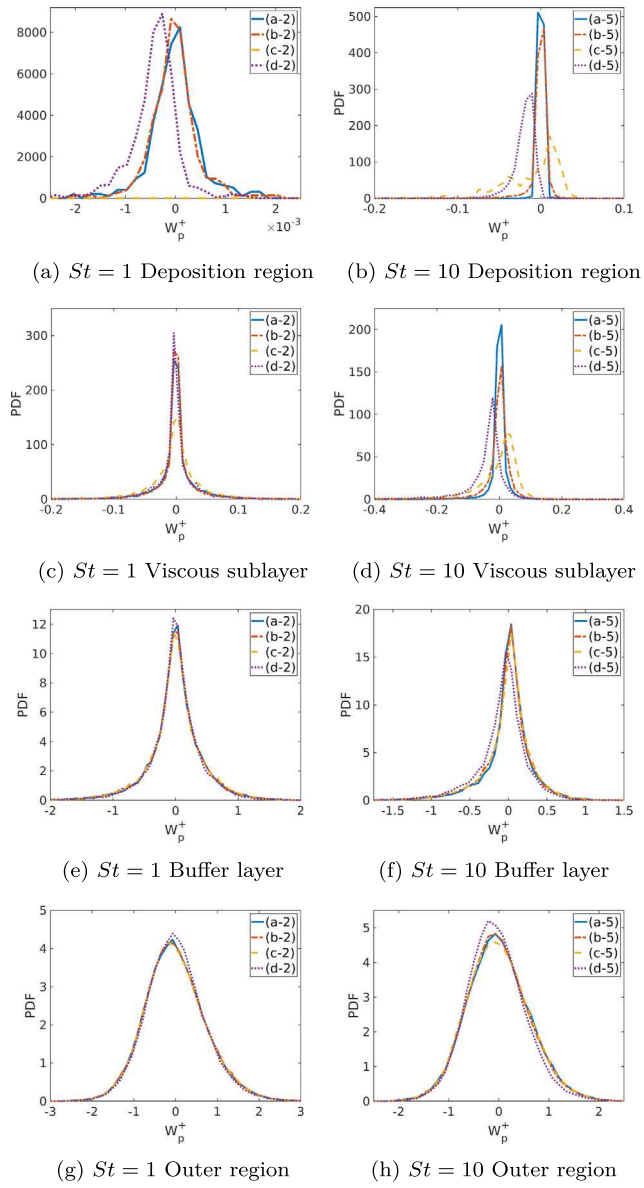

(a) $St = 1$ Deposition region (b) $St = 10$ Deposition region

(c) $St = 1$ Viscous sublayer (d) $St = 10$ Viscous sublayer

(e) $St = 1$ Buffer layer (f) $St = 10$ Buffer layer

(g) $St = 1$ Outer region (h) $St = 10$ Outer region

Fig. 18. Pdf of wall-normal velocity in different layers for (a), (c), (e), (g) case (*-2) and (b), (d), (f), (h) case (*-5). Buffer layer and outer region are almost homogeneous, the magnitude and direction of particle wall-normal velocity changes with including different accelerations.

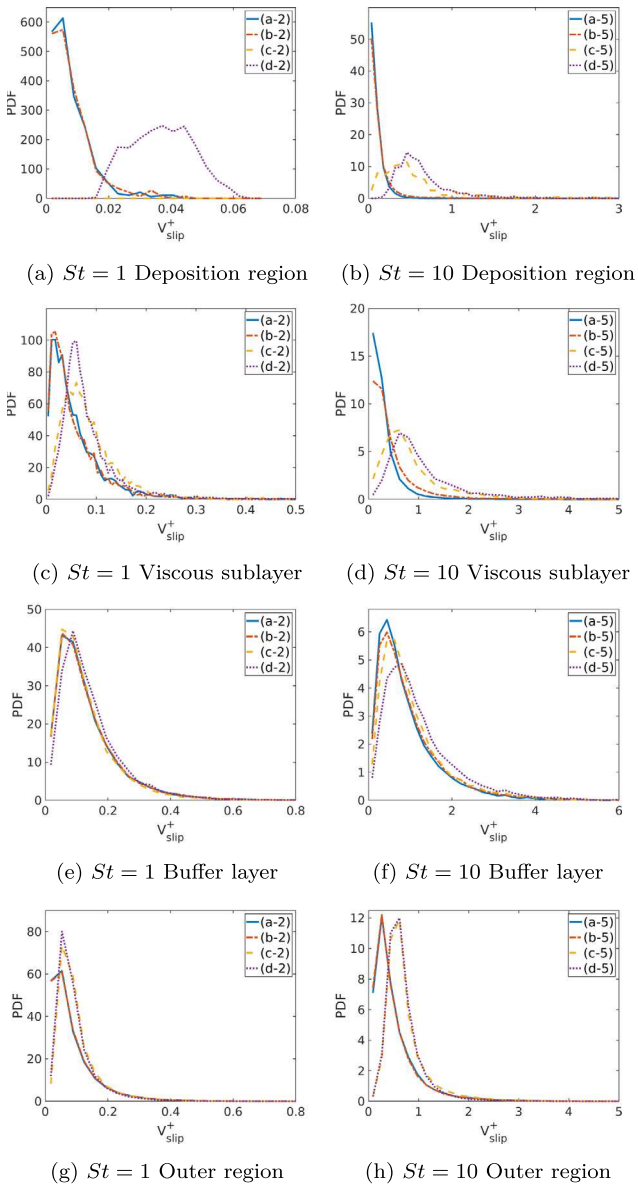

(a) $St = 1$ Deposition region (b) $St = 10$ Deposition region

(c) $St = 1$ Viscous sublayer (d) $St = 10$ Viscous sublayer

(e) $St = 1$ Buffer layer (f) $St = 10$ Buffer layer

(g) $St = 1$ Outer region (h) $St = 10$ Outer region

Fig. 19. Pdf of magnitude of slip velocity in different layers for (a), (c), (e), (g) case (*-2) and (b), (d), (f), (h) case (*-5). Including gravity changes the slip velocity significantly.

and downward flow. As mentioned before, this change in slip velocity alters the wall-normal lift acceleration which can be different for each particle. Additionally, even small amount of lift near the wall can have strong impulses on deposition rate since the fluid wall-normal velocity is almost zero at the wall. Therefore, the determining factors for obtaining particle deposition are particle size and density as well as the included forces.

5. Conclusion

The objective of this work was to study dynamics of particle deposition and explore whether the Stokes number solely is enough to describe the deposition or other quantities such as particle size and density need to be considered. Therefore, we aimed to obtain the deposition rate for various sizes and densities with the same Stokes numbers. Thus, we performed several PP-DNSs for different combinations of particle sizes and particle to fluid density ratios at the same Stokes number (detailed in Table 1). The simulations were carried out in a turbulent channel flow at $Re_\tau = 180$.

In this work, we could draw two main conclusions; (1) Stokes number alone cannot be used to describe the deposition velocity/rate. In particular, particle size and property as well as fluid phase characteristics need to be considered. (2) Accounting for gravity and lift accelerations is of a great importance when studying deposition. Consistent with findings of McLaughlin (1989), it turned out even a small amount of lift very close to the wall (where fluid wall-normal velocity drops to nearly zero) alter the deposition rate remarkably. Gravity alters the deposition process substantially by modifying the particle slip velocity and as a result lift in wall-normal direction, consistent with conclusion of Brandt and Coletti (2022). However, the change in the deposition rate due to gravity and lift is a function of the Stokes number, particle size, density as well as direction of the flow.

It is also worth noting that the wall boundary corrections on drag proposed by Faxen (1923) and Maude (1965) and lift by Takemura and

Magnaudet (2003) were considered in our studies, which have non-negligible effects (results without such corrections are not shown for the sake of brevity) on the deposition dynamics.

Moreover, our results demonstrate that the particle velocity variance plays an important role to control the deposition process, at least for the ranges of particle sizes considered here. Therefore, the obtained results provide useful indications required to further develop more accurate models such as stochastic acceleration models introduced by Lattanzi et al. (2020) that aim at capturing particle velocity variance accurately.

Finally, we would like to mention that this study considers only the effect of particle characteristics (size and density) on the deposition at a constant fluid Reynolds number. However, as shown by Bernardini (2014), the deposition rate is also dependent on flow characteristics (fluid Reynolds number).

CRediT authorship contribution statement

S. Abbasi: Conceptualization, Data curation, Formal analysis, Methodology, Software, Validation, Visualization, Writing – original draft, Writing – review & editing. **A. Mehdizadeh:** Conceptualization, Funding acquisition, Investigation, Project administration, Resources, Supervision, Writing – original draft, Writing – review & editing.

Declaration of competing interest

The authors declare the following financial interests/personal relationships which may be considered as potential competing interests: Amirfarhang Mehdizadeh reports financial support was provided by American Chemical Society and National Science Foundation Division of Chemical, Bioengineering, Environmental and Transport Systems (CBET). Sanaz Abbasi reports equipment, drugs, or supplies was provided by ACCESS.

Data availability

Data will be made available on request.

Acknowledgments

This work is supported by the American Chemical Society under grant "PRF# 61817–ND9" and the National Science Foundation CBET, Award # 2219446. Additionally, the computational time was provided by NCSA Delta CPU at University of Illinois Urbana–Champain and Rockfish at Johns Hopkins University through allocation "MCH220032" from the Advanced Cyberinfrastructure Coordination Ecosystem: Services & Support (ACCESS) program, which is supported by National Science Foundation grants # 2138259, #2138286, #2138307, #2137603, and #2138296. Finally, we thank Pedro Costa for his guidance and insights in developing PP-CaNS code.

References

Alcoforado, L., Ari, A., Barcelar, J.d., Brandão, S.C.S., Fink, J.B., de Andrade, A.D., 2019. Impact of gas flow and humidity on trans-nasal aerosol deposition via nasal cannula in adults: A randomized cross-over study. Pharmaceutics 11 (7), 320.

Alimohammadi, S., Zendehboudi, S., James, L., 2019. A comprehensive review of asphaltene deposition in petroleum reservoirs: Theory, challenges, and tips. Fuel 252, 753–791.

Arcen, B., Tanière, A., Oesterlé, B., 2006. On the influence of near-wall forces in particle-laden channel flows. Int. J. Multiphas. Flow 32 (12), 1326–1339.

Bernardini, M., 2014. Reynolds number scaling of inertial particle statistics in turbulent channel flows. J. Fluid Mech. 758, R1.

Brandt, L., Coletti, F., 2022. Particle – Laden turbulence: Progress and perspectives. Annu. Rev. Fluid Mech. 54 (1), 159–189.

Bui, V.K.H., Moon, J., Chae, M., Park, D., Lee, Y., 2020. Prediction of aerosol deposition in the human respiratory tract via computational models: A review with recent updates. Atmosphere-Basel 11 (2), 137.

Cai, Y., Tay, K., Zheng, Z., Yang, W., Wang, H., Zeng, G., Li, Z., Siah, K.B., Subbaiah, P., 2018. Modeling of ash formation and deposition processes in coal and biomass fired boilers: A comprehensive review. Appl. Energ. 230, 1447–1544.

Chauhan, V., 2019. Superheated Steam Scrubbing and Utilization for Power Generation (Ph.D. thesis). Reykjavik University, Iceland.

Chauhan, V., Gudjonsdottir, M., Saevarsdottir, G., 2020. Silica particle deposition in superheated steam in an annular flow: Computational modeling and experimental investigation. Geothermics 86, 101802.

Chen, M., McLaughlin, J.B., 1995. A new correlation for the aerosol deposition rate in vertical ducts. J. Colloid Interf. Sci. 169 (2), 437–455.

Costa, P., 2018. A FFT-based finite-difference solver for massively-parallel direct numerical simulations of turbulent flows. Comput. Math. Appl. 76 (8), 1853–1862.

Dance, S., Maxey, M., 2003. Incorporation of lubrication effects into the force–coupling method for particulate two–phase flow. J. Comput. Phys. 189 (1), 212–238.

Faxen, H., 1923. Die Bewegung einer starren Kugel langs der Achse eines mit zaher Flussigkeit gefullten Rohres. Arkiv for Mat. Astron. Fys. 17, 1–28.

Fong, K.O., Amili, O., Coletti, F., 2019. Velocity and spatial distribution of inertial particles in a turbulent channel flow. J. Fluid Mech. 872, 367–406.

Friedlander, S.K., Johnstone, H.F., 1957. Deposition of suspended particles from turbulent gas streams. Ind. Eng. Chem. 49 (7), 1151–1156.

Gharbi, K., Benyounes, K., Khodja, M., 2017. Removal and prevention of asphaltene deposition during oil production: A literature review. J. Petrol. Sci. Eng. 158, 351–360.

Guha, A., 2008. Transport and deposition of particles in turbulent and laminar flow. Annu. Rev. Fluid Mech. 40 (1), 311–341.

Healy, D., Young, J., 2010. An experimental and theoretical study of particle deposition due to thermophoresis and turbulence in an annular flow. Int. J. Multiphas. Flow 36 (11), 870–881.

Johnson, P.L., Bassenne, M., Moin, P., 2020. Turbophoresis of small inertial particles: Theoretical considerations and application to wall-modelled large-eddy simulations. J. Fluid Mech. 883, A27.

Kaftori, D., Hetsroni, G., Banerjee, S., 1995. Particle behavior in the turbulent boundary layer. II. Velocity and distribution profiles. Phys. Fluids 7 (5), 1107–1121.

Kleinhans, U., Wieland, C., Frandsen, F.J., Spliethoff, H., 2018. Ash formation and deposition in coal and biomass fired combustion systems: Progress and challenges in the field of ash particle sticking and rebound behavior. Prog. Energ. Combust. 68, 65–168.

Kuerten, J.G.M., 2006. Subgrid modeling in particle-laden channel flow. Phys. Fluids 18 (2), 025108.

Kurz, R., Brun, K., 2012. Fouling mechanisms in axial compressors. J. Eng. Gas Turb. Power 134 (3), 032401.

Lattanzi, A.M., Tavanashad, V., Subramaniam, S., Capecelatro, J., 2020. Stochastic models for capturing dispersion in particle–laden flows. J. Fluid Mech. 903, A7.

Lu, H., Wang, Y., 2019. Particle deposition in ventilation ducts: A review. Build. Simul.–China 12, 723–734.

Marchioli, C., Picciotto, M., Soldati, A., 2007. Influence of gravity and lift on particle velocity statistics and transfer rates in turbulent vertical channel flow. Int. J. Multiphas. Flow 33 (3), 227–251.

Marchioli, C., Soldati, A., 2002. Mechanisms for particle transfer and segregation in a turbulent boundary layer. J. Fluid Mech. 468, 283–315.

Marchioli, C., Soldati, A., Kuerten, J., Arcen, B., Tanière, A., Goldensoph, G., Squires, K., Cargnelutti, M., Portela, L., 2008. Statistics of particle dispersion in direct numerical simulations of wall-bounded turbulence: Results of an international collaborative benchmark test. Int. J. Multiphas. Flow 34 (9), 879–893.

Maude, A.D., 1965. The movement of a sphere in front of a plane at low Reynolds number. Br. J. Appl. Phys. 14 (12), 894.

McLaughlin, J.B., 1989. Aerosol particle deposition in numerically simulated channel flow. Phys. Fluids A-Fluid 1 (7), 1211–1224.

McLaughlin, J.B., 1991. Inertial migration of a small sphere in linear shear flows. J. Fluid Mech. 224, 261–274.

Mei, R., 1992. An approximate expression for the shear lift force on a spherical particle at finite reynolds number. Int. J. Multiphas. Flow 18 (1), 145–147.

Molin, D., Marchioli, C., Soldati, A., 2012. Turbulence modulation and microbubble dynamics in vertical channel flow. Int. J. Multiphas. Flow 42, 80–95.

Monchaux, R., Bourgoin, M., Cartellier, A., 2010. Preferential concentration of heavy particles: A Voronoïanalysis. Phys. Fluids 22 (10), 103304.

Mortimer, L.F., Njobuenwu, D.O., Fairweather, M., 2019. Near-wall dynamics of inertial particles in dilute turbulent channel flows. Phys. Fluids 31 (6), 063302.

Narayanan, C., Lakehal, D., Botto, L., Soldati, A., 2003. Mechanisms of particle deposition in a fully developed turbulent open channel flow. Phys. Fluids 15 (3), 763–775.

Ounis, H., Ahmadi, G., McLaughlin, J.B., 1991. Brownian diffusion of submicrometer particles in the viscous sublayer. J. Colloid Interf. Sci. 143 (1), 266–277.

Paes, D., Ribeiro, P., Shirdel, M., Sepehrnoori, K., 2015. Study of asphaltene deposition in wellbores during turbulent flow. J. Petrol. Sci. Eng. 129, 77–87.

Rousta, F., Lessani, B., Ahmadi, G., 2023. Particle dispersion and deposition in wall-bounded turbulent flow. Int. J. Multiphas. Flow 158, 104307.

Saffman, P.G., 1965. The lift on a small sphere in a slow shear flow. J. Fluid Mech. 22 (2), 385–400.

Santos, B., 2009. Corrosion and fouling in petrochemical environments. In: NACE CORROSION, pp. NACE–09163.
Sardina, G., Schlatter, P., Brandt, L., Picano, F., Casciola, C.M., 2012. Wall accumulation and spatial localization in particle-laden wall flows. J. Fluid Mech. 699, 50–78.
Schiller, L., Naumann, Z., 1935. A drag coefficient correlation. Z. Ver. Deutsch. Ing. 77 (318), 318–320.
Sehmel, G.A., 1968. Aerosol Deposition from Turbulent Airstreams in Vertical Conduits. AEC Research & Development Report, Battelle Northwest Lab., Richland, Washington, USA.
Shi, P., Rzehak, R., 2020. Lift forces on solid spherical particles in wall-bounded flows. Chem. Eng. Sci. 211, 115264.
Soldati, A., Marchioli, C., 2009. Physics and modelling of turbulent particle deposition and entrainment: Review of a systematic study. Int. J. Multiphas. Flow 35 (9), 827–839, Special Issue: Point-Particle Model for Disperse Turbulent Flows.
Soltani, M., Ahmadi, G., 1995. Direct numerical simulation of particle entrainment in turbulent channel flow. Phys. Fluids 7 (3), 647–657.
Sommerfeld, M., Sgrott, O., Taborda, M., Koullapis, P., Bauer, K., Kassinos, S., 2021. Analysis of flow field and turbulence predictions in a lung model applying RANS and implications for particle deposition. Eur. J. Pharm. Sci. 166, 105959.
Takemura, F., Magnaudet, J., 2003. The transverse force on clean and contaminated bubbles rising near a vertical wall at moderate Reynolds number. J. Fluid Mech. 495, 235–253.
Vasseur, P., Cox, R.G., 1977. The lateral migration of spherical particles sedimenting in a stagnant bounded fluid. J. Fluid Mech. 80 (3), 561–591.
Xiao, W., Jin, T., Luo, K., Dai, Q., Fan, J., 2020. Eulerian-Lagrangian direct numerical simulation of preferential accumulation of inertial particles in a compressible turbulent boundary layer. J. Fluid Mech. 903, A19.
Young, J., Leeming, A., 1997. A theory of particle deposition in turbulent pipe flow. J. Fluid Mech. 340, 129–159.
Zhang, H., Ahmadi, G., 2000. Aerosol particle transport and deposition in vertical and horizontal turbulent duct flows. J. Fluid Mech. 406, 55–80.